A NOVEL EMBEDDED INLET BASED ON THE INTEGRATED DESIGN CONCEPT OF FUSELAGE AND INLET

Yan Panpan[1], Liu Fangliang[2]

[1] Shenyang Aircraft Design and Research Institute , ShenYang, China
[2] Shenyang Aircraft Design and Research Institute, Chinese Aeronautical Establishment, ShenYang, China

Abstract

To improve the performance and applicable Mach number of the submerged inlet, a novel submerged inlet combined with pre-compression forebody is designed based on forebody/inlet integration design concept. Composing different flow direction and spanwise geometric parameters of the forebody, multiple inlet models are built up. The performance and flow characteristic of different cases is obtained by numerical simulation. The effect of forebody geometric parameters on the inlet performance is further studied. The results indicate that spanwise compression has a major impact on the total pressure recovery and distortion coefficient of the inlet. For Ma=0.6, at the design condition, the total pressure recovery coefficient increases by 0.04 and reaches 0.98, the applicable Mach number expands from 0.6 to 0.75 compared with the baseline case. Performance of the submerged inlet is improved by using the pre-compression of the forebody.

Keywords: Submerged Inlet; CFD; Total Pressure Recovery; Distortion Index; Integrated Design

1. General Introduction

The submerged inlet has no exposed structure protruding from the surface, which makes the aircraft more compact. It can effectively reduce the radar cross section (RCS) of the inlet, and has excellent stealth performance. At the same time, it can significantly reduce the wind drag resistance of the aircraft [1]. As early as the 1940s, Frick et al designed a NACA submerged inlet, and carried out a lot of design and experimental research on it [2-7]. Subsequently, it gradually developed from the initial auxiliary inlet to the main inlet and successfully applied to the AGM-129 cruise missile, Tacit Blue stealth technology verification aircraft and MQ-25 UAV. However, due to the lack of effective use of the inflow ram pressure, the submerged inlet has some technical difficulties, such as large distortion index and low total pressure recovery coefficient, and with the increase of Mach number, the performance of the inlet decreases more seriously [8].

In order to improve the performance of the inlet and expand the range of available Mach number, a new submerged inlet was designed based on the integrated design idea of inlet and fuselage. The influence of the front body surface parameters on the inlet performance was studied by numerical simulation method.

2. Methodology

2.1 Governing Equations

The governing equations are three-dimensional compressible Navier-Strokes equations.

$$\frac{\partial}{\partial t}\int_{\Omega} W d\Omega + \oint_{\partial\Omega}\left(F_e - F_v\right)dS = \int_{\Omega} Q d\Omega$$

where W denotes conservative variables, F_c represents the vector of the convective fluxes, F_v stands for the vector of viscous fluxes, Q is the source term, Ω denotes control volume, and dS represents surface element. The conservative variables.

$$W = \begin{bmatrix} \rho & \rho u & \rho v & \rho w & \rho E \end{bmatrix}^T$$

where ρ, u, v, w, E denote the density, the Cartesian velocity components and the total energy per unit mass, respectively. The vector of the convective fluxes F_c on dynamic grids can be written as

$$F_c = \begin{bmatrix} \rho V \\ \rho u V + n_x p \\ \rho v V + n_y p \\ \rho w V + n_z p \\ \rho H V \end{bmatrix}$$

where V is the contravariant velocity, p denotes static pressure, and H is total enthalpy.

$$V \equiv \vec{v} \cdot \vec{n} = n_x u + n_y v + n_z w$$

$$H = E + \frac{p}{\rho}$$

where V is velocity vector, g represents the grid velocity, and n_x, n_y, n_z denote the components of the outward facing unit normal vector of the surface $\partial\Omega$, respectively. Furthermore,

$$F_v = \begin{bmatrix} 0 \\ n_x \tau_{xx} + n_y \tau_{xy} + n_z \tau_{xz} \\ n_x \tau_{yx} + n_y \tau_{yy} + n_z \tau_{yz} \\ n_x \tau_{zx} + n_y \tau_{zy} + n_z \tau_{zz} \\ n_x \Theta_x + n_y \Theta_y + n_z \Theta_z \end{bmatrix}$$

$$Q = \begin{bmatrix} 0 \\ \rho f_{e,x} \\ \rho f_{e,y} \\ \rho f_{e,z} \\ \rho f_e \cdot v + \dot{q}_h \end{bmatrix}$$

where $\tau_{ij}(i=x,y,z;j=x,y,z)$ represents viscous stress, f_e denotes the body force, $f_{e,x}, f_{e,y}, f_{e,z}$ are the three components of f_e, $\dot{}$ is heat fluxes density [9].

The governing equations were solved by the cell-centered finite-volume method, where the convective terms were computed by the second-order upwind scheme and the viscous flux terms by a central-difference method. The least-squares gradient reconstruction method with the modified Venkatakrishnan gradient reconstruction limiter was used.

2.2 SST k-ω method

The turbulence model SST (Shear Stress transport) is based on two equations. This model manages calculations of both k-ω and k-ε thus tackling adverse pressure gradients and turbulence properties. The transport equation in transitional SST model is governed by the flowing equation [10-12].

$$\frac{\partial \rho k}{\partial t} + \nabla \cdot \left(\rho k \vec{U} \right) - \nabla \left[\left(\mu + \sigma_{k1} \mu_t \right) \nabla k \right] + P_k - C_\mu \rho k \omega$$

$$\frac{\partial \rho \omega}{\partial t} + \nabla \cdot \left(\rho \omega \vec{U} \right) - \cdot \left[\left(\mu + \sigma_{\omega 1} \mu_t \right) \nabla \omega \right] + 2 \left(1 - F_1 \right) \rho \sigma_{\omega 2} \frac{\nabla k \cdot \nabla \omega}{\omega} + \rho \alpha \mathbf{S}^2 - \beta \rho \omega^2$$

$$\mu_t = \frac{a_1 k}{\max \left(a_1 \omega, F_2 \mathbf{S} \right)}$$

$$F_1 = \tanh\left\{ \left[\min\left(\max\left(\frac{\sqrt{k}}{C_\mu \omega y}, \frac{500\nu}{y^2 \omega} \right), \frac{4\rho\sigma_{\omega 2}k}{D_{k\omega}y^2} \right) \right]^4 \right\} \quad D_{k\omega} = \max\left(2\rho\sigma_{\omega 2} \frac{\nabla k \cdot \nabla \omega}{\omega}, 10^{-10} \right)$$

$$F_2 = \tanh\left[\left[\max\left(\frac{2\sqrt{k}}{C_\mu \omega y}, \frac{500\nu}{y^2 \omega} \right) \right]^2 \right]$$

where y is the distance to the wall.

$$P_k = \min\left(\mu_t S^2, 10 \cdot C_\mu \rho k \omega \right), C_\mu = 0.09$$

where $\alpha_1 = 5/9, \beta_1 = 3/40, \sigma_{k1} = 0.85, \sigma_{\omega 1} = 0.85 \quad \alpha_2 = 0.44, \beta_2 = 0.0828, \sigma_{k2} = 1, \sigma_{\omega 2} = 0.856$

2.3 Validation

An S-duct case is considered here to evaluate the accuracy of our numerical method. Figure 2 gives the geometry of the S-duct inlet, where R is the ratio of the center line. θ_{max} represents the angle of the arc, φ is the central angle of the cross section and r_1/r_2 is the radius of the inlet and oulet of the intake.
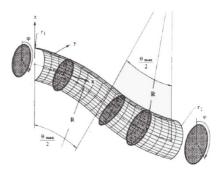

Figure 1 – Sketch of S-duct [13]

The inflow Mach number is 0.6, and Reynolds number based on the inlet diameter. The flow characteristic of the inlet is simulated and Figure 2 gives the secondary flow sketch of the outlet cross section[14-16]. A pair of vortex structure caused by the cross pressure gradient is clearly shown in the picture.
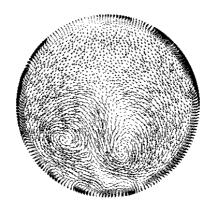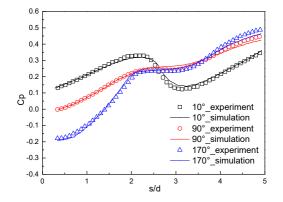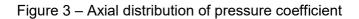

Figure 2 – Computed secondary flow in outlet cross section

The pressure coefficient distribution of different circumferential angle $\phi = 10°$, $\phi = 90°$, $\phi = 170°$ is obtained and compared with the experimental result as shown in Figure3. s represents the length of the centerline away from the inlet, d is the diameter of the inlet cross section. Close inspections reveals a good match among numerical simulation and experiments results, which demonstrates the reliability and the accuracy of the CFD method in predicting the flow characteristics of the inlet flow.

Figure 3 – Axial distribution of pressure coefficient
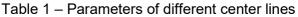
3. Computational and Analysis

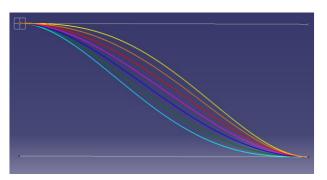### 3.1 The design and characteristics of baseline inlet

In order to obtain the basic performance of submerged inlet, a submerged inlet is designed on a flat plate and some main design parameters are studied. Firstly, the influence of center lines are studied. The formula is as follows:
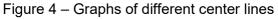
$$Y = A\left(\frac{x}{L}\right)^2 + B\left(\frac{x}{L}\right)^3 + C\left(\frac{x}{L}\right)^4$$

By changing the values of coefficients A, B, and C, different center line types can be obtained. Table 1 shows the parameter values of 7 different center lines from front to back, and graphs of center lines are shown in Figure 4.

Table 1 – Parameters of different center lines

order	A	B	C
C1	-3	4	0
C2	-2	2	1
C3	-1	0	2
C4	0	-2	3
C5	1	-4	4
C6	2	-6	5
C7	3	-8	6

Figure 4 – Graphs of different center lines

According to the above center line, seven different 2-D submerged pressure inlets were established. Two dimensional CFD simulation was carried out to obtain the influence of different center lines. Their geometry and mesh are shown in Figure 5.
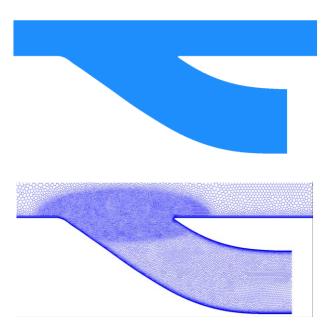
4

Figure 5 – The geometry and mesh of 2-D submerged inlet

Figure 6 shows the flow field simulation results of seven center line schemes with Mach numbers of 0.2, 0.4 and 0.6. It can be seen that with the increase of Mach number, the separation area in the inlet increases, and the flow field gradually deteriorates. For example 6 and 7, when the Mach number reaches 0.4 and above, the flow is separated throughout the whole pipe. Considering both high speed and low speed performances, C3 is chosen as the reference center line.

Figure 6 – Velocity vector diagram of different baseline inlet under different Mach numbers

Then the intake shape was studied. The lip shape of the submerged inlet is designed under irregular pentagonal shape and is parameterized by 9 variables. The lip shape is shown in Figure 7. Through parametric selection design, the geometry of intake shaped of the baseline inlet is obtained, as
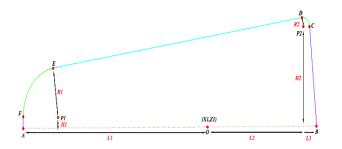
shown in Figure 8.

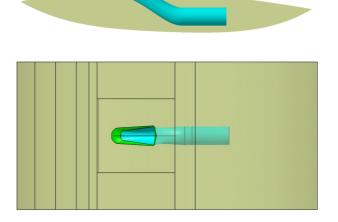Figure 7 – Parametric shape of intake lip of submerged inlet

Figure 8 – The 3-D shape of submerged inlet

A numerical simulation method was used to evaluate the performance of the baseline inlet, and the inlet aerodynamic characteristics were simulated at Ma=0.2, 0.4 and 0.6. The intake flow characteristics were simulated by changing the outlet back pressure of the inlet. Figure 9 and Figure 10 show the distribution of the surface and volume mesh.
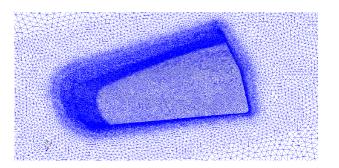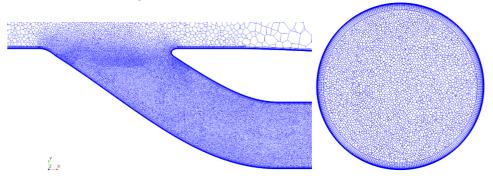

Figure 9 The surface mesh of the inlet

Figure 10 The body mesh of the inlet

6

Figure 11 illustrates the comparisons of the total pressure recovery coefficient between the baseline submerged inlet and the conventional inlet under different Mach numbers. It can be seen that the submerged inlet has a very good performance at low speed, when the total pressure recovery coefficient is more than 5% higher than that of the conventional inlet, which is equivalent to about 7% increase in installation thrust. However, as the Mach number increases, the total pressure recovery coefficient decreases dramatically. This becomes even more severe for high angle of attack, as shown in Figure 12. Figure 13 gives the vector velocity of symmetric surface for Ma=0.6.To solve this problem, assistant control system should be used for high angle of attack and high Mach number in order to improve the high speed performances.
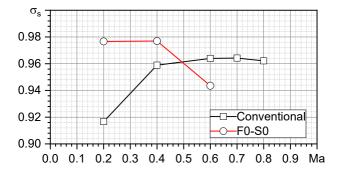

Figure 11 – The performances of different types of inlet under different Mach numbers
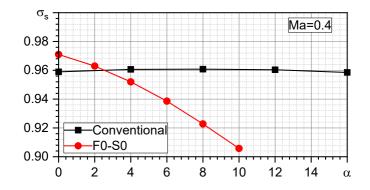

Figure 12 – The performances of different types of inlet under different angles of attack
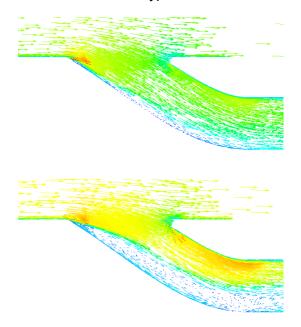

Figure 13 – Vector velocity of symmetric surface (Ma=0.6)

3.2 Design of New Inlet

Based on the previous study, it was found that the shape of the fuselage has a significant effect on the performance of the submerged inlet. In order to clarify the influence of the forebody on inlet aerodynamic characteristics, a detailed study was carried out. The flow direction and spanwise parameters is considered as the key design parameters. Figure14 shows the different profiles of the parameter, which is represented by F0 to F4 and S0 to S4.
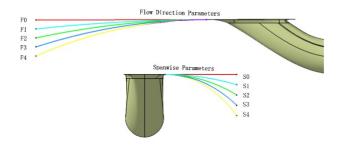

Figure 14 – Flow direction and spanwise design parameters

A variety of fusion schemes of precursor and submerged inlet were designed by changing the parameters of the flow direction and the span wise profile of the precursor, as shown in Figure15.

Firstly, the separate effects of flow direction parameter and spanwise parameter are studied by simulation method. According to the results, some special combinations of the two parameters were further studied.
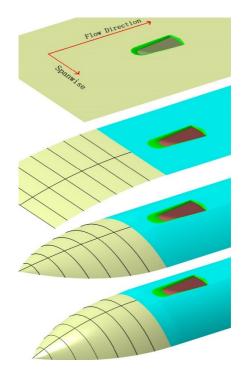

Figure 15 – Sketch of the inlet models

3.3 Simulation Result and Analysis

The three dimensional Reynolds averaged Navier-Stokes equations and Menter SST turbulent model equations were solved to simulate the flow characteristics and performance of these inlets.

3.3.1 Effect of Flow Direction Parameter

The influence of different flow direction design parameters on the submerged inlet total pressure recovery coefficient is shown in Figure 16. It shows that with the increase of the flow direction shape curvature the total pressure recovery coefficient first rises and then falls, the inlet with flow direction parameter F2 gives the best performance and the total pressure recovery coefficient can reach $\sigma s=0.96$.

Figure 17 shows the total pressure recovery coefficient distributions of inlet cross section for case F0_S0 and F2_S0, the position of the section is illustrated in Figure 18. As can be seen the low pressure recovery area is concentrated on the lower surface of the inlet. This is caused by the flow separation near the lower surface. By changing the flow direction shape curvature of the fuselage, the low pressure recovery area is decreased which leads to the increase of the inlet performance.
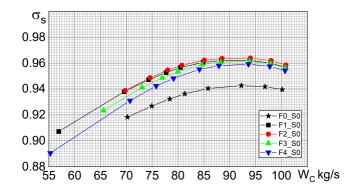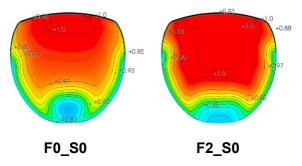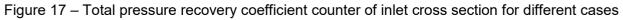

Figure 16 – Total pressure recovery coefficient for different flow direction design parameters
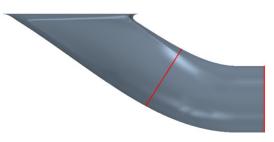

F0_S0   **F2_S0**

Figure 17 – Total pressure recovery coefficient counter of inlet cross section for different cases

Figure 18 – Schematic diagram of section position

3.3.2 Effect of Flow Direction Parameter

The influence of span wise design parameters on submerged inlet total pressure recovery coefficient is illustrated in Figure 19. Similar to the influence of flow direction parameters, with the increase of spanwise shape curvature the total pressure recovery coefficient first rises and then falls. The inlet with spanwise parameter S1 gives the best performance and the total pressure recovery coefficient can nearly reach σ_s=0.97.

The performance of the inlet which is obtained by changing the spanwise parameter is better than those inlets obtained by changing the flow direction parameter.
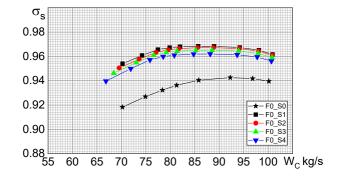
Figure 19 – Total pressure recovery coefficient for different span wise design parameters

Figure 20 shows the velocity vector distribution of inlet symmetrical plane for case F0_S0 and F0_S1. Compared with the baseline case F0_S0, changing the spanwise shape curvature of the fuselage can significantly decrease the separation area near the lower surface of the inlet and diminish the total pressure lose caused by flow separation.
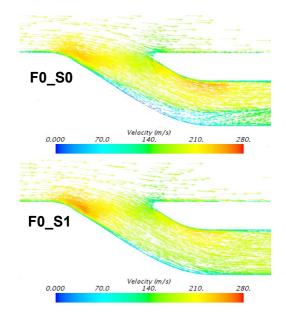

Figure 20 – Velocity vector distribution of inlet symmetrical plane for different cases (Ma=0.6)

3.3.3 Result for the Combinations of the Two Parameters

Figure 21 gives the total pressure recovery coefficient for different flow direction and span wise design parameter combinations. As can be seen the combination of different parameters can further increase the performance of the inlet, for the combination of F3 and S3, the total pressure recovery coefficient can nearly reach σ_s=0.98.
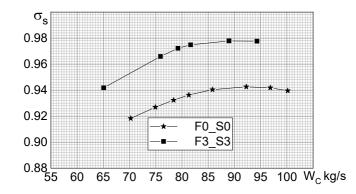

Figure 21 – Total pressure recovery coefficient for different parameter combinations

4. Conclusions

To improve the performance of a submerged inlet, a novel submerged inlet is designed based on the integration design concept of fuselage and inlet. Composing different flow direction and spanwise geometric parameters of the forebody, multiple inlet models are built up and the performance is obtained by numerical simulation. The results indicate that changing shape curvature of the fuselage can decrease the separation near the lower surface in the duct and increase the performance of the inlet.

5. Contact Author Email Address

All authors contributed equally.

Corresponding author: Panpan Yan, Email address: yanpp816@126.com

Tel:+86 024-86361221; Fax:+86 024-86360409

Mailing address: Tawan Street 40, Huanggu District, Shenyang, LiaoNing Province, China

6. Copyright Statement

References

[1] D.S. Cheng, S. Sun, Y.F. Wen, et al, "Submerged inlet performance improvement with bellowing on fuselage", Journal of Aerospace Power, 27, 1131-1138, (2012).

[2] C.W. Frick, W.F. Davis, L.M. Randall, "An experimental investigation of NACA submerged duct entrances", NACA ACR, 5I20, (1945).

[3] C.F. Hall, J.L Frank, "Ram-recovery characteristics of NACA submerged inlets at high subsonic speeds", NACA RM-A8I29, (1948).

[4] W.E. Anderson, A.C. Frazer, "Investigation of an NACA submerged inlet at Mach numbers from 1.17 to 1.99", NACA RM-A52F17, (1952).

[5] J. Seddon, E.L. Smith, "Intake Aerodynamics", [M]. London：Blackwell Science Ltd, 338—340, (1999).

[6] Taskinoglu E S, Knighty D. Numerical analysis of sub-merged inlets [R]. AIAA-2002-3147, (2002).

[7] Dovey J R, Subsonic drag and pressure recovery of rectangular planform flush auxiliary inlets with ducts at angles up to 90 degrees [R]. The Royal Aeronautical Society, ESDU 03006, (2003).

[8] J.X. Che, W. Ye, H.T. Sun, "Experimental Investigation of a Full-Scale Submerged Inlet in Ground Runnin", Gas Turbine Experiment and Research, 27, 12-15, (2014).

[9] Blazek J.Computational fulid dynamics principles and applications. [M].London：Elsevier, 16-18, (2005).

[10]Menter F R. Two-equation eddy-viscosity turbulence models for engineering applications [J]. AIAA journal, 32(8): 1598-1605, (1994).

[11]Menter F R, Kuntz M, Langtry R. Ten years of industrial experience with the SST turbulence model [J]. Turbulence, heat and mass transfer, 4(1) , (2003).

[12]Menter F R, Kuntz M. Adaptation of Eddy Viscosity Turbulence Models to Unsteady Separated Flow Behind Vehicles [J]. The Aerodynamics of Heavy Vehicles: Trucks, Buses, and Trains, 19: 339, (2004).

[13]Wellborn S R, Reichert B A, Okiishi T H. An experimental investigation of the flow in a diffusing S-duct [C]// Proceedings of 28th Joint Propulsion Conference and Exhibit.Nashville: NASA:1-13, (1992).

[14]LIU zhenxia, GUO Dongming, ZHANG Lifen,et al. Numerical simulation of flow field for supersonic S-shap inlet[J]. Journal of Aerospace Power, 21(6): 1064-1068, (2006).

[15]WONG Xiaochai, GUO Rongwei. Investigation of pneumatic characteristics for a ventral S-shaped inlet at high incidence and low speed [J]. Journal of Aerospace Power, 23(9): 1573-1578, (2008).

[16]XIE Wenzhong,GUO Rongwei. Flow field of ventral diverterless high offset S-shaped inlet at transonic speeds[J]. Acta Aeronautica et Astronautica Sinica, 29(6):1453-1459, (2008).